International Journal of Heat and Mass Transfer 186 (2022) 122431

Contents lists available at ScienceDirect

International Journal of Heat and Mass Transfer

journal homepage: www.elsevier.com/locate/hmt

Validity of performance factors used in recent studies on heat transfer enhancement by surface modification or insert devices

Siti Nurul Akmal Yusof[a], Nura Mu'az Muhammad[b,c], Wan Mohd Arif Aziz Japar[b], Yutaka Asako[b,*], Chungpyo Hong[d], Lit Ken Tan[b], Nor Azwadi Che Sidik[b]

[a] Faculty of Innovative Design and Technology, Universiti Sultan Zainal Abidin, Kampus Gong Badak, 21300 Kuala Nerus, Terengganu Darul Iman, Malaysia
[b] Department of Mechanical Precision Engineering, Malaysia-Japan International Institute of Technology, University Technology Malaysia, Jalan Sultan Yahya Petra, 54100 Kuala Lumpur, Malaysia
[c] Faculty of Engineering, Kano University of Science and Technology, Wudil, Nigeria
[d] Department of Mechanical Engineering, Kagoshima University, 1-21-40 Korimoto, Kagoshima, 890-8580, Japan

ARTICLE INFO

Article history:
Received 13 September 2021
Revised 6 December 2021
Accepted 13 December 2021
Available online 30 December 2021

Keyword:
Performance factor
Heat transfer enhancement
Validity
Baffle plate

ABSTRACT

Based on literature survey, the performance factors were used in 62 articles which have been published in 2021 in International Journal of Heat and Mass Transfer, International communications in Heat and Mass Transfer, International Journal of Thermal Sciences and Applied Thermal Engineering, to evaluate the heat transfer enhancement by geometry modification or insertion of tapes, wires or turbulence promoters under identical pumping power. However, the validity of the performance factors was not examined yet. The heat transfer rate in a periodic fully developed region of a circular duct with periodic annular baffle plates was numerically obtained. Comparing the heat transfer rate with that of a circular smooth duct, the validity of the performance factors used in previous studies was examined. It was found that the performance factors used in the previous studies are not valid for the evaluation of heat transfer enhancement. Furthermore, this paper shows that the direct comparison of heat transfer rates without the assumptions of equal surface area and the equal temperature difference is suitable for the evaluation of heat transfer enhancement.

1. Introduction

There have been many demands to enhance the forced convection heat transfer because of its wide application. Geometry or surface modifications such as interrupted fins or surface roughness, and insertion of tapes, wires or turbulence promoters have been introduced as passive techniques. Webb and Eckert [1] proposed the following performance factor for evaluating heat transfer enhancement of the flow in a circular duct with ribs under an identical pumping power.

$$\eta = \frac{\dot{Q}}{\dot{Q}_s} = \frac{hA\,\Delta t}{[hA\,\Delta t]_s} \approx \frac{Nu}{Nu_s} = \frac{St/St_s}{\mathrm{Re}_s/\mathrm{Re}} = \frac{St/St_s}{(f/f_s)^{1/3}} \tag{1}$$

Eq. (1) expresses the ratio of the heat transfer rates of flows in a ribbed duct and in a smooth surface duct. The Reynolds number ratio in Eq. (1) is replaced by the friction factor ratio using the correlation between the Reynolds numbers of the ribbed and the smooth ducts. Under the identical pumping power, the Reynolds number of the smooth duct is expressed by the Reynolds number of the ribbed duct as

$$\mathrm{Re}_s = (f/f_s)^{1/3}\,\mathrm{Re} \tag{2}$$

Note that Eq. (1) was derived under the assumptions of $A = A_s$ & $\Delta t = \Delta t_s$ since the heat transfer rate ratio, $\dot{Q}/\dot{Q}_s$, was approximated by the Nusselt number ratio.

Since the Stanton number is expressed as $St = Nu/(\mathrm{Re\ Pr})$ and the Prandtl number is identical, the ratio of the Stanton numbers can be replaced by the Nusselt number ratio if we assume $\mathrm{Re} = \mathrm{Re}_s$. Then, Eq. (1) can be rewritten as

$$\eta = \frac{Nu/Nu_s}{(f/f_s)^{1/3}} \tag{3}$$

where Nu_s and f_s are the Nusselt number and the friction factor of the smooth duct at Re_s defined by Eq. (2). Although, it is not clearly described, many researchers seemed to calculate the performance factor from the following equation.

$$\eta = \frac{Nu/Nu_s^*}{(f/f_s^*)^{1/3}} \tag{4}$$

* Corresponding author.
E-mail address: y.asako@utm.my (Y. Asako).

https://doi.org/10.1016/j.ijheatmasstransfer.2021.122431
0017-9310/

Nomenclature

A	surface area, m^2
C_p	specific heat , W/(kg K)
D	diameter of a circular duct, m
f	Darcy friction factor, -
h	cycle average heat transfer coefficient, W/(m^2 K)
k	thermal conductivity, W/(m K)
L	pitch of annular baffle plates, m
$\dot{m}$	mass flow rate, kg/s
Nu	cycle average Nusselt number, -
N_X, N_R	numbers of grids in X- and R-directions, -
p	pressure, Pa
p'	periodic pressure, Pa
Δp	pressure drop per unit length, Pa
Pr	Prandtl number, -
$\dot{Q}$	heat transfer rate, W
r_i, r_o	inner and outer radii of annular plate, m
Re	Reynolds number, -
St	Stanton number, -
t	temperature, K
t_b, t_w	bulk and wall temperatures, K
Δt	temperature difference, K
T	dimensionless temperature, -
u, v	velocity components, m/s
$\bar{u}$	average velocity, m/s
U, V	dimensionless velocity components, -
$\bar{U}$	dimensionless average velocity, -
$\dot{V}$	volume flow rate, m^3/s
x, r	coordinates, m
X, R	dimensionless coordinates, -
Greek	
β	per-cycle pressure gradient, Pa/m
γ	bulk-to-wall temperature ratio, 1/m^2
Γ	dimensionless bulk-to-wall temperature ratio, -
η	performance factor, -
λ	bulk-temperature-gradient parameter, 1/m
Λ	dimensionless bulk-temperature-gradient parameter, -
μ	viscosity, Pa s
ν	kinematic viscosity, m^2/s
θ	dimensionless bulk temperature based on t_w and t_{in}, -
$\dot{\Theta}$	dimensionless heat transfer rate, -
ρ	density, kg/m^3
subscript	
b	duct with baffle plates
in	inlet
max	maxium
n	cycle number
s	smooth surface

where Nu_s^* and f_s^* are the Nusselt number and the friction factor of the smooth duct at $Re_s = Re$ [2]. Note that the assumption of $Re = Re_s$ is physically inconsistent, since the Reynolds numbers for a smooth duct and for a modified surface duct are different under the identical pumping power. However, many researchers have used Eq. (3) or Eq. (4) to evaluate the heat transfer enhancement of modification of surfaces [e.g. 3–10].

Some researchers obtained the following performance factor to evaluate heat transfer enhancement [e.g. 11,12].

$$\eta = \frac{Nu/Nu_s}{(\Delta p/\Delta p_s)^{1/3}} \tag{5}$$

Eq. (5) is the equation whose denominator is replaced by the pressure loss ratio. However, there is the following correlation under the identical pumping power.

$$\Delta p \, Re = \Delta p_s \, Re_s \tag{6}$$

Therefore, substituting Eqs. (2) and (6) into Eq. (3), Eq. (3) can be rewritten as

$$\eta = \frac{Nu/Nu_s}{\Delta p/\Delta p_s} \tag{7}$$

Eq. (7) and Eq. (3) are identical equation. Lv et al. [13] used Eq. (7) for the evaluation of the heat transfer enhancement. Note that the performance factors expressed by Eqs. (1) and (3-4) are derived as the indicators with many assumptions under the identical pumping power. In contrast, Asako and Faghri [14] directly compared the heat transfer rates of the corrugated duct and the parallel plates duct under the identical pumping power, the identical pressure drop and the identical mass flow rates. However, Eqs. (1) and (3-4) still have been used to evaluate the heat transfer enhancement by modifying the heat transfer surface.

Here, a question arises whether Eqs. (1) and (3-4) are valid for evaluating heat transfer enhancement by modifying the heat transfer surface because of the assumptions in derivation. However, the literature survey failed to find any prior work which investigates the validity of Eqs. (1) and (3-4). Only the exception is our previous study which investigated whether Eq. (3) was valid for evaluating heat transfer enhancement by using a nanofluid [15]. The validity of Eq. (3) was verified by comparing the heat transfer rate ratio of the nanofluid flow and the base fluid flow in a circular smooth duct and the value obtained from Eq. (3). The heat transfer rates were obtained from the empirical correlations and experimental data obtained from previous studies. It was found that Eq. (3) used in the previous studies is not suitable for evaluating heat transfer enhancement by nanofluids. This has motivated the present study to examine the validity of Eqs. (1) and (3-4) for flows in a circular duct with periodic annular circular baffle plates.

2. Formulation

2.1. Description of the sample problem

The validation was conducted on heat transfer in a periodic fully developed region of a circular duct with periodic annular baffle plates. The problem to be considered in this study is depicted schematically in Fig. 1. The circular duct wall is heated with constant wall temperature. The geometry of the problem is specified by the duct diameter (D), the inner radius of the annular plate (r_i), the outer radius (r_o), and the pitch of the annular plates (L). The annular baffle plate is negligible thin. With the assumption of periodic fully developed flow, the solution domain is confined to a typical module shaded in Fig. 1. As described by Patankar et al. [16], the periodic fully developed flow is characterized by a velocity field that repeats itself at corresponding axial stations in successive cycles. Furthermore, in such a regime, the pressures of

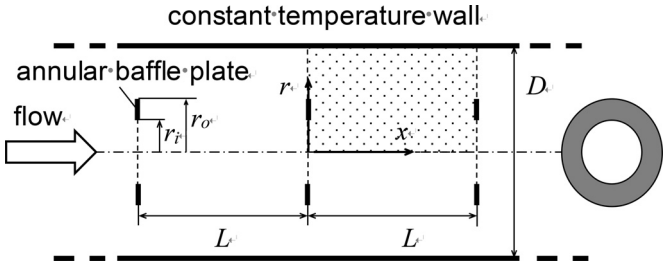

Fig. 1. Schematic diagram of circular duct with annular baffle plates.

cyclically corresponding locations decrease linearly in the downstream direction. The pressure, p is expressed by

$$p(x,r) = -\beta x + p'(x,r) \tag{8}$$

where β is a constant, and $p'(x,r)$ behaves in a periodic manner from plate to plate. The term $-\beta x$ represents the non-periodic pressure drop that takes place in the flow direction.

For a case of uniform wall temperature boundary condition, the fluid temperature approaches the wall temperature in the periodically fully developed region. Therefore, the following dimensionless temperature will be introduced.

$$T(x,r) = \frac{t(x,r) - t_w}{t_b - t_w} \tag{9}$$

where t_b is the bulk temperature and

$$t_b - t_w = \frac{\int r(t - t_w)\,|u|\,dr}{\int r|u|\,dr} \tag{10}$$

In the periodic thermally developed region, the dimensionless temperature satisfies the following relationship:

$$T(x,r) = T(x+L,r) = T(x+2L,r) = \cdots \tag{11}$$

Therefore, the fully developed dimensionless temperature field repeats itself at corresponding axial stations in successive cycles.

2.2. Conservation equations

The flow in the duct is assumed to be steady, laminar and two-dimensional. Because of its symmetric nature, flow physics variation in the circumferential direction is negligible. All the fluid properties are assumed to be constant. Under these assumptions, the continuity and the momentum equations can be expressed as:

$$\frac{\partial u}{\partial x} + \frac{1}{r}\frac{\partial rv}{\partial r} = 0 \tag{12}$$

$$\frac{\partial uu}{\partial x} + \frac{1}{r}\frac{\partial rvu}{\partial r} = -\frac{1}{\rho}\frac{\partial p'}{\partial x} + \nu\left\{\frac{\partial^2 u}{\partial x^2} + \frac{1}{r}\frac{\partial}{\partial r}\left(r\frac{\partial u}{\partial r}\right)\right\} + \frac{\beta}{\rho} \tag{13}$$

$$\frac{\partial uv}{\partial x} + \frac{1}{r}\frac{\partial rvv}{\partial r} = -\frac{1}{\rho}\frac{\partial p'}{\partial r} + \nu\left\{\frac{\partial^2 v}{\partial x^2} + \frac{1}{r}\frac{\partial}{\partial r}\left(r\frac{\partial v}{\partial r}\right) - \frac{v}{r^2}\right\} \tag{14}$$

The energy equation for the constant wall temperature case is expressed as

$$\frac{\partial uT}{\partial x} + \frac{1}{r}\frac{\partial rvT}{\partial r} = \frac{k}{\rho C_p}\left\{\frac{\partial^2 T}{\partial x^2} + \frac{1}{r}\frac{\partial}{\partial r}\left(r\frac{\partial T}{\partial r}\right)\right\} + \frac{k}{\rho C_p}\gamma \tag{15}$$

where $\gamma = (\lambda^2 + \frac{d\lambda}{dx})T + 2\lambda\frac{\partial T}{\partial x} - \frac{\lambda}{k/(\rho C_p)}uT$ and

$$\lambda = \frac{d(t_b - t_w)/dx}{t_b - t_w} \tag{16}$$

Using the following dimensionless variables:

$X = \frac{x}{D}$, $R = \frac{r}{D}$, $U = \frac{uD}{\nu}$, $V = \frac{\nu D}{\nu}$, $P = \frac{p'}{\rho\,(\nu/D)^2}$,

$T(x,r) = \frac{t(x,r)-t_w}{t_b-t_w}$, $B = \frac{\beta D^3}{\rho\,\nu^2}$, $\Gamma = D^2\,\gamma$, $\Lambda = D\,\lambda$,

$$\dot{\Theta} = \frac{\dot{Q}}{k\,D\,(t_w - t_b)_{in}},\ \mathrm{Re} = \frac{\bar{u}D}{\nu} = \bar{U},\ \mathrm{Pr} = \frac{\nu}{k/(\rho C_p)} \tag{17}$$

The dimensionless forms of the governing equations can be expressed as follows:

$$\frac{\partial U}{\partial X} + \frac{1}{R}\frac{\partial RV}{\partial R} = 0 \tag{18}$$

$$\frac{\partial UU}{\partial X} + \frac{1}{R}\frac{\partial RVU}{\partial R} = -\frac{\partial P}{\partial X} + \left\{\frac{\partial^2 U}{\partial X^2} + \frac{1}{R}\frac{\partial}{\partial R}\left(R\frac{\partial U}{\partial R}\right)\right\} + B \tag{19}$$

$$\frac{\partial UV}{\partial X} + \frac{1}{R}\frac{\partial RVV}{\partial R} = -\frac{\partial P}{\partial R} + \left\{\frac{\partial^2 V}{\partial X^2} + \frac{1}{R}\frac{\partial}{\partial R}\left(R\frac{\partial V}{\partial R}\right) - \frac{V}{R^2}\right\} \tag{20}$$

The energy equation for the constant wall temperature case is expressed as

$$\frac{\partial UT}{\partial X} + \frac{1}{R}\frac{\partial RVT}{\partial R} = \frac{1}{\mathrm{Pr}}\left\{\frac{\partial^2 T}{\partial X^2} + \frac{1}{R}\frac{\partial}{\partial R}\left(R\frac{\partial T}{\partial R}\right)\right\} + \frac{\Gamma}{\mathrm{Pr}} \tag{21}$$

where $\Gamma = (\Lambda^2 + \frac{d\Lambda}{dX})T + 2\Lambda\frac{\partial T}{\partial X} - \mathrm{Pr}\,\Lambda\,U\,T$ and

$$\Lambda = \frac{d(t_b - t_w)/dX}{t_b - t_w} \tag{22}$$

$\Lambda$is a periodic function of X arising from the assumptions of the constant wall temperature boundary condition. Substituting dimensionless variables into Eq. (10), Eq. (10) is rewritten as

$$\frac{\int RT|U|\,dR}{\int R\,|U|\,dR} = 1 \tag{23}$$

The dimensionless temperature for the constant wall temperature case should satisfy Eq. (23). $\Lambda$is determined by satisfying Eq. (23) as a part of the solution process.

2.3. Boundary conditions

To complete the formulation of the problem in the physical domain, it remains to discuss the boundary conditions. These are non-slip condition on the wall including the baffle plates and periodic conditions at the inlet and outlet ends of the solution domain. Since the baffle plate is negligible thin, there is no need to consider the thermal resistance and the thermal capacitance of the plate. The dimensionless boundary conditions are expressed as:

at the inlet and outlet (periodic condition):

$U_{X=0} = U_{X=L/D}$, $(\partial U/\partial X)_{X=0} = (\partial U/\partial X)_{X=L/D}$,

$V_{X=0} = V_{X=L/D}$, $(\partial V/\partial X)_{X=0} = (\partial V/\partial X)_{X=L/D}$

$T_{X=0} = T_{X=L/D}$, $(\partial T/\partial X)_{X=0} = (\partial T/\partial X)_{X=L/D}$

on the wall $(R = 0.5)$: $\quad U = V = 0, \quad T = 0$

on the symmetric line $(R = 0)$:

$\partial U/\partial X = 0, \quad V = 0, \quad \partial T/\partial R = 0$

on the annular baffle plate : $\quad U = V = 0$ (24)

Friction Factor, Pumping Power, Heat Transfer Rate and Nusselt Number

Attention will now be focused on the calculation of the friction factor which will be defined as

$$f = \frac{-(dp/dx)\,D}{\frac{1}{2}\rho\,\bar{u}^2} = \frac{2B}{\bar{U}^2} = \frac{2B}{\mathrm{Re}^2} \tag{25}$$

Another quantity of interest is the pumping power. The dimensionless pumping power per unit length is defined as

$$\frac{\Delta p\dot{V}}{\frac{\pi}{4}\frac{\rho\,\nu^3}{D}} = B\,\mathrm{Re} \tag{26}$$

where $\Delta p$is the pressure drop per unit length, $\dot{V}$ is the volume flow rate and $\Delta p\dot{V}$ represents the pumping power per unit length. In the case of the identical pumping power, the dimensionless form of the relation $(\Delta p\dot{V})_b = (\Delta p\dot{V})_s$ is expressed as

$$(B\,\mathrm{Re})_b = (B\,\mathrm{Re})_s \tag{27}$$

The mass flow rate, $\dot{m}$, is expressed as $\dot{m} = (\pi/4)\,\mu\,D\,\mathrm{Re}$. In the case of the identical mass flow, the following correlation is obtained.

$$\mathrm{Re}_b = \mathrm{Re}_s \tag{28}$$

Note that Eq. (28) is also available in the case of the identical volume flow rate. The subscript b and s represent ducts with baffle plates and smooth surface. Since B represents the dimensionless pressure gradient, the following correlation is obtained under the identical pressure drop.

$$B_b = B_s \tag{29}$$

The cycle average Nusselt number is defined by

$$Nu = \left(\frac{\dot{Q}/A_w}{\overline{t_w - t_b}} \right) \frac{D}{k} \tag{30}$$

where $A_w = \pi\, D\, L$ is the heat transfer surface area and $\dot{Q}$ is the per-cycle heat transfer rate of the flow in the circular duct with periodic annular baffles and is calculated from the temperature gradient at the wall as

$$\dot{Q} = \pi\, D \int_0^L k \left(\frac{\partial\, t}{\partial\, r} \right)_{D/2} dx \tag{31}$$

$\overline{t_w - t_b}$ is the log mean temperature difference and is expressed by

$$\overline{t_w - t_b} = (t_w - t_b)_{in} \frac{1 - \exp\left(\int_0^{L/D} \Lambda\, dX \right)}{-\int_0^{L/D} \Lambda\, dX} \tag{32}$$

Substituting Eqs. (31) and (32) and the dimensionless variables into Eq. (30), the cycle average Nusselt number is rewritten as

$$Nu = \frac{1}{L/D} \frac{\int_0^{L/D} \Lambda\, dX}{1 - \exp\left(\int_0^{L/D} \Lambda\, dX \right)} \times \int_0^{L/D} \exp\left(\int_0^X \Lambda\, dX \right) \left(\frac{\partial T}{\partial R} \right)_{R=0.5} dX \tag{33}$$

The cycle average Nusselt number was calculated from Eq. (33). In the periodic thermally fully developed region, the cycle average Nusselt number value of each cycle is identical. To confirm this, supplementary computations were conducted for two cases where the computational domain was extended to two cycles and three cycles from the single cycle. The obtained average Nusselt numbers of two cycles and three cycles are identical to that of the single cycle. The dimensionless heat transfer rate of a cyclic duct of n-cycles is expressed as [15, 17]

$$\dot{\Theta}_n = \frac{\dot{Q}_n}{k\, D\, (t_w - t_b)_{in}} = \frac{\pi}{4} \mathrm{Re}\ \mathrm{Pr} \left\{ 1 - \exp\left(\frac{-4\, Nu}{\mathrm{Re}\ \mathrm{Pr}} \frac{nL}{D} \right) \right\} \tag{34}$$

where n is a natural number ($n = 1,\ 2,\ 3,\ \cdots$). The dimensionless heat transfer rate of a cyclic duct of n-cycles was calculated from Eq. (34).

2.4. Computational parameters for sample computation

From an examination of the governing equations in Eqs. (18)-(22), it can be seen that there are two parameters whose values have to be specified prior to the initiation of the numerical computation. These are the Prandtl number, Pr, and the dimensionless per-cycle pressure gradient, B. In this paper, $\mathrm{Pr} = 5$ is selected assuming that the fluid is water. The values chosen for B is selected in such a way that the calculated Reynolds number ranges from 50 to 500. Aside from the Pr and B, there are three geometric parameters which have to be specified. Since the diameter of the duct D is chosen for the reference length, the geometric parameters are the pitch of the baffle plates and diameter ratio, L/D, the dimensionless inner and outer radii of the annular baffle plate, r_i/D and r_o/D. The selected values of these parameters are $L/D = 5$, $r_i/D = 0.1$ and $r_o/D = 0.2$.

The attention will turn to the computational range of the Reynolds number. The flow behind the annular baffle plate is an unsteady flow or a turbulent flow when the Reynolds number is high. Twin vortices are observed in a flow behind a cylinder in the range of $10 < \mathrm{Re}_{cyl} < 40$ where Re_{cyl} is the Reynolds number based on the cylinder diameter. In the range of $\mathrm{Re}_{cyl} > 40$, the flow transitions to the unsteady laminar flow [18]. The height of the baffle plate, $r_o - r_i$, is 0.1 D. The Reynolds number based on the height of the baffle plate is a tenth of Reynolds number of the duct flow. Although the annular baffle plate is not a cylinder, we assumed that the flow in the range of the Reynolds number from 50 to 500 is a steady laminar flow.

2.5. Numerical method

The discretization procedure of the governing equations is based on the control volume based power law scheme of Patankar [19]. The pressure and velocity are linked by the SIMPLE algorithm of Patankar [19]. The convergence criterion used in this computation was that the value of the mass flux residuals (mass flow) divided by the total mass flow in each control volume took a value under 10^{-13}. A non-uniform grid distribution with a high concentration near the inlet, the outlet, the edges of the annular baffle plate and the wall. They were a structured grid . A typical grid distribution for a case of $N_X = 1000$ and $N_R = 200$ is shown in Fig. 2. The grid size in the X-direction was gradually increased from the inlet to the mid and it gradually decreased to the outlet in a power-law spacing fashion [20]. The grid size in the R-direction was gradually decreases from the center to the inner edge of the annular baffle plate. It was gradually increased and decreased between the inner and outer edges of the baffle plate and between the outer edge and the wall in a power-law spacing fashion. The selected indexes of the power-law spacing in X-direction and R-direction were 1.4. The computational time depends on the dimensionless pressure gradient, B. The computational time for $B = 30000$ with the grids of $N_X = 1000$ and $N_R = 200$ was 3.2 h by a personal computer with Intel core i7–4770 K 3.50 GHz processor. The corresponding Reynolds number is 439.

2.6. Grid size effect

The effect of number of grids in R-direction on the cycle average Nusselt number was examined. $B = 16{,}000$ was chosen for the dimensionless pressure gradient and its corresponding Reynolds number is about 260. The results are tabulated in Table 1. The number of the grids in X-direction is fixed at 400. N_1, N_2 and N_3 are numbers of the grids from the center to the inner edge, from the inner edge to the outer edge, and from the outer edge to the wall and N_R is the sum of them. As can be seen from this table, the grid size effect on Nu_m decreases with increasing the number of the grids. Then, $N_R = 200$was chosen for the number of the grids in R-direction.

The effect of number of the grids in X-direction on the cycle average Nusselt number was also examined for N_X=400, 600, 800 and 1000. $B = 16{,}000$ was chosen for the dimensionless pressure gradient and its corresponding Reynolds number is about 261. The number of the grids in R-direction was fixed at 200. The Nu is plotted in Fig. 3 as a function of the inverse of N_X. The dashed line is the curve fitted line obtained from the Nu of N_X=400, 600, 800 and 1000. The Nu decreases almost linearly with decreasing $1/N_X$, then, the value of Nu at $1/N_X = 0$ was obtained by extrapolation of the curve fitted line. Supplementary runs for N_X=1200, 1600 and 2000 were conducted and the results coincide with the curve fitted line obtained from the Nu of N_X=400, 600, 800 and 1000. Then, the cycle average Nusselt number was obtained in such away that Nu of N_X=400, 600, 800 and 1000 were obtained first. Next, they

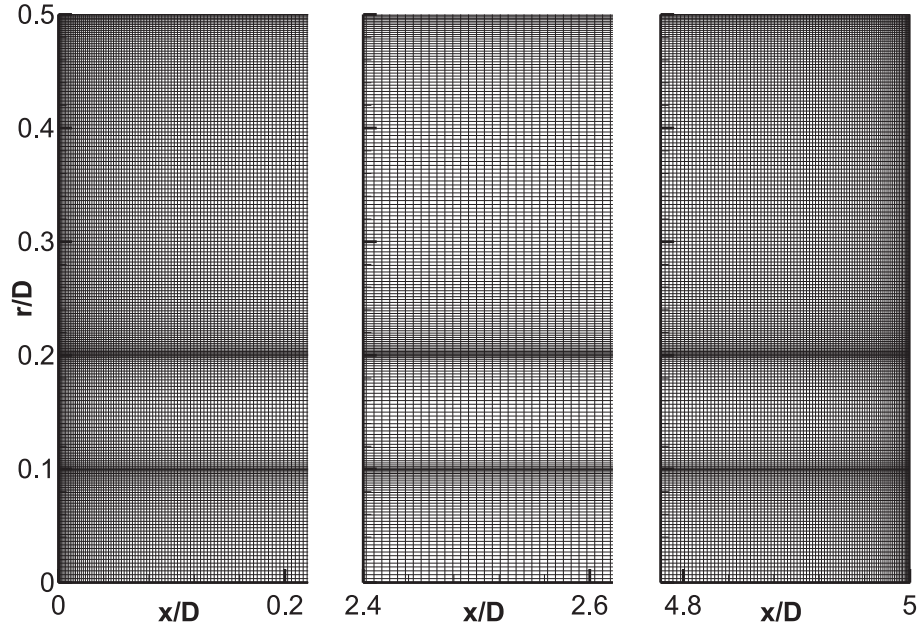

Fig. 2. A typical grid distribution ($N_X = 1000$, $N_R = 200$).

Table 1
Grid size effect.

N_X	N_1 (R = 0–0.1)	N_2 (R = 0.1–0.2)	N_3 (R = 0.2–0.5)	N_R	Nu	$\frac{Nu-Nu_{N_R=250}}{Nu_{N_R=250}} \times 100$
400	10	10	30	50	4.9593	7.24%
	20	20	60	100	4.7229	2.13%
	30	30	90	150	4.6609	0.79%
	40	40	120	200	4.6363	0.26%
	50	50	150	250	4.6243	–

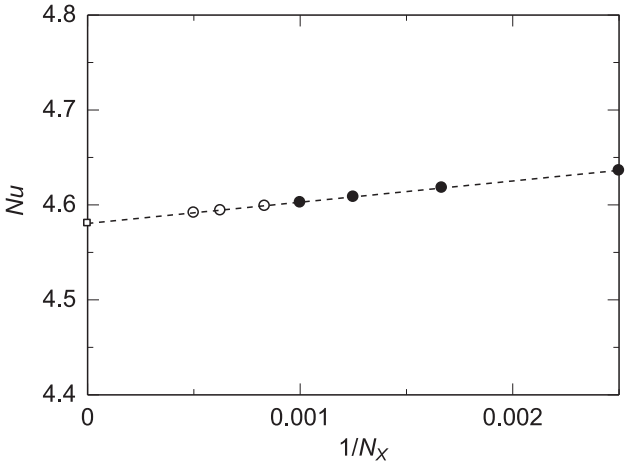

Fig. 3. Grid size effect on cycle average Nu at B = 16,000.

were plotted as a function of $1/N_X$ and the curve fitted line was obtained. The value of Nu at $1/N_X = 0$ was determined by the extrapolation of the curve fitted line.

3. Results and discussion

Sample computations were conducted for the case of $\mathrm{Pr} = 5$, $L/D = 5$, $r_1/D = 0.1$ and $r_2/D = 0.2$. The streamline map obtained from the solution for B = 30,000 is presented in Fig. 4(a). The corresponding Reynolds number is 438.5. The blue small lines at $X = 0$ and $X = 5$ are the annular baffle plates. The flow direction changes to the wall by the annular baffle plate. Vortices can be seen behind the annular baffle plate. The contour plot of dimensionless temperatures, T, in the tube is presented in Fig. 4(b). Since the dimensionless temperatures, T, is defined by Eq. (9), T at the wall takes 0 on the wall and the dimensionless bulk temperature takes unity. The boundary layer in the range from $X = 0$ to $X = 0.7$ becomes thin because of the flow.

The correlations between Re_s and Re_b under the identical pressure drop, the identical pumping power and the identical mass flow rate are plotted in Fig. 5. Since the analytical value of the $f\,\mathrm{Re}$ of the smooth circular duct is 64, substituting this value into Eq. (25) the dimensionless pressure gradient B of the smooth circular duct is expressed as

$$B_s = 32\,\mathrm{Re}_s \tag{35}$$

Substituting Eq. (35) into Eq. (27), the Reynolds number of the smooth circular duct under the identical pumping power is obtained as

$$\mathrm{Re}_s = \left\{\frac{1}{32}\,(B\,\mathrm{Re})_b\right\}^{1/2} \tag{36}$$

Substituting Eq. (35) into Eq. (29), the Reynolds number of the smooth circular duct under the identical pressure drop is obtained as

$$\mathrm{Re}_s = \frac{B_b}{32} \tag{37}$$

Since the dimensionless pressure gradient B is the computational parameter, the Reynolds number of a duct with baffle plates, Re_b, is obtained for a specified B_b after solving the flow field. Substituting these B_b and Re_b into Eq. (36), the Reynolds number of

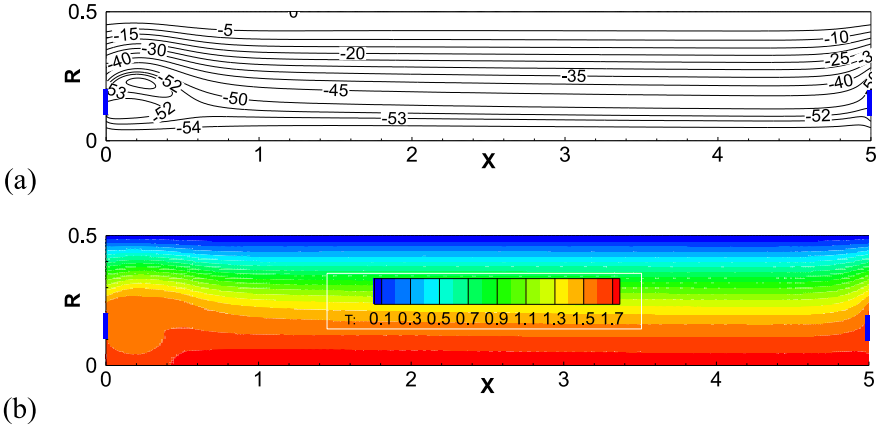

Fig. 4. (a) Stream lines (b) T contour at $B = 30{,}000$ ($\mathrm{Re}_b = 438.5$).

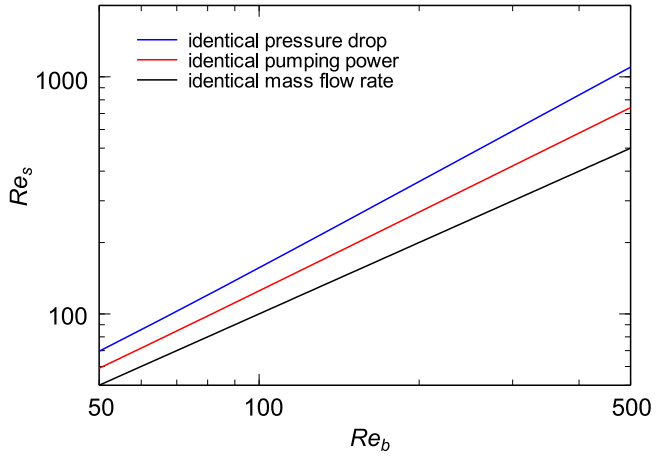

Fig. 5. Correlations between Re_s and Re_b under typical flow constraints.

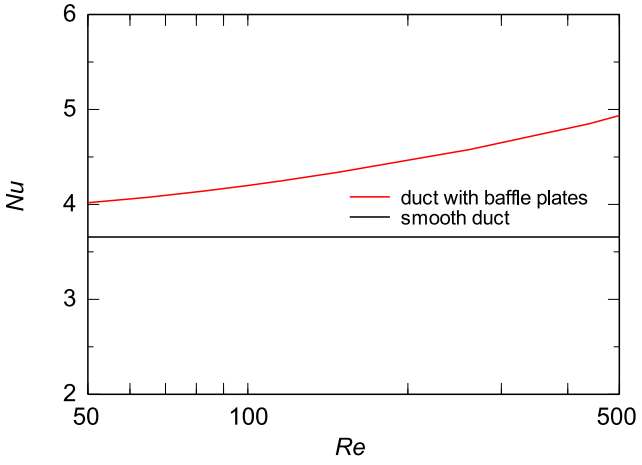

Fig. 7. Cycle average Nusselt number.

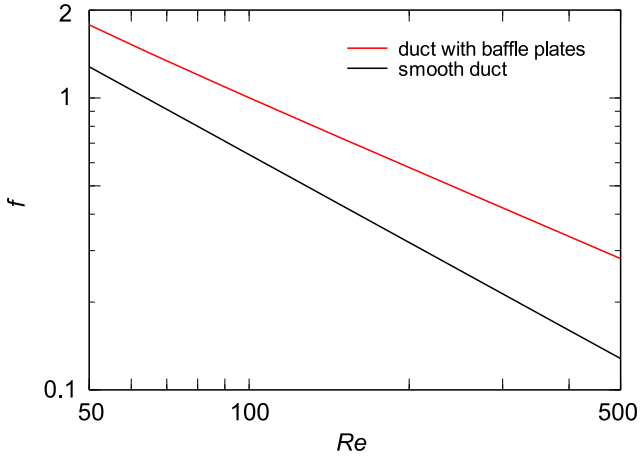

Fig. 6. Friction factor as a function of Re.

the smooth duct under the identical pumping power, Re_s, is obtained. In the case of the identical pressure drop, substituting B_b into Eq. (37), the correlation between Re_s and Re_b is obtained. As can be seen from the figure, the difference between Re_s and Re_b is large under the identical pressure drop.

The friction factors of the smooth circular duct and the circular duct with the periodic annular baffle plates are plotted in Fig. 6. The friction factor of the circular duct with the baffle plates is 1.4 to 2.1 times higher than that of the smooth duct.

The cycle average Nusselt number of the smooth circular duct and the circular duct with the periodic annular baffle plates are plotted in Fig. 7. Although the Nusselt number of the smooth circular duct in the thermally fully developed region is constant ($Nu = 3.6568$), the cycle average Nusselt number of the circular duct with the baffle plates increases with increasing the Re number.

The heat transfer rate of the 50 cyclic duct with the periodic baffle plates calculated from Eq. (34) is plotted in Fig. 8. Since the L/D of one cycle is 5, the total length of the 50 cyclic duct is 250 D. The heat transfer rate of the smooth circular duct of 250 D is also plotted in Fig. 8. As seen from the figure that he heat transfer rate of the 50 cyclic duct with the periodic baffle plates is higher than that of the smooth circular duct of the same length. The heat transfer rate ratio is greater than unity under the identical mass flow rate.

3.1. Performance factor

Here, we will consider the performance factor for the evaluation index of the heat transfer enhancement of flows in ducts with constant wall temperature. The performance factor, which is a heat transfer rates ratio defined as the following equation is suitable for the evaluation index in the case of the constant wall temperature.

$$\eta = \frac{\dot{Q}_{b,n}}{\dot{Q}_{s,n}} = \frac{\dot{\Theta}_{b,n}}{\dot{\Theta}_{s,n}} \tag{38}$$

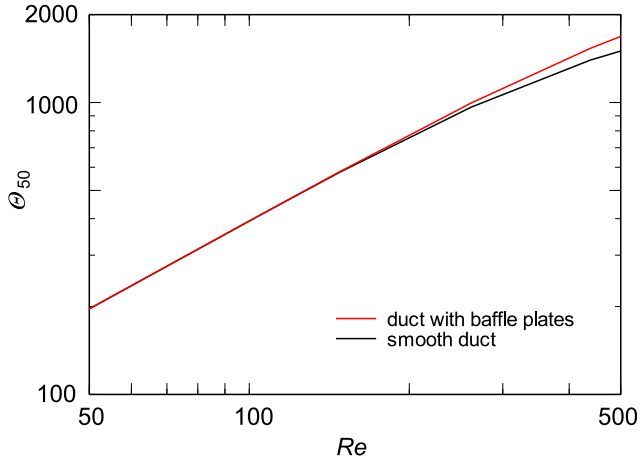

Fig. 8. Heat transfer rate of 50 cyclic duct.

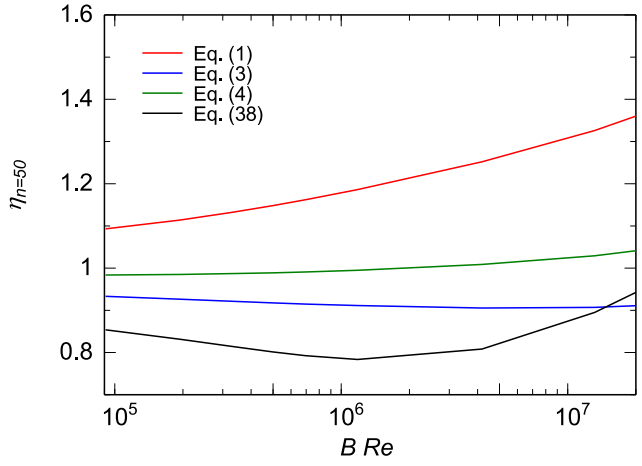

Fig. 9. Performance factor of 50 cyclic duct under identical pumping power.

where $\dot{\Theta}_{b,n}$ and $\dot{\Theta}_{s,n}$ are the dimensionless heat transfer rates of a cyclic duct of n cycles with periodic baffles and a smooth circular duct which are calculated from Eq. (34).

3.2. Identical pumping power

The performance factors of the 50 cyclic duct calculated from Eqs. (1), (3), (4) and (38) under an identical pumping power are plotted in Fig. 9 as a function of the dimensionless pumping power per unit length defined in Eq. (26). As seen in the figure, there are discrepancies between the performance factors calculated from Eqs. (1), (3) and (4) and the value calculated from Eq. (38). The performance factor calculated from Eq. (1) gives a higher performance factor value. Therefore, the performance factors calculated from Eqs. (1), (3) and (4) are not appropriate for the evaluation of the heat transfer enhancement under the identical pumping power.

The average Nusselt number and the friction factor of the smooth duct in the hydrodynamically and thermally fully developed region are constant. The cycle average Nusselt number of the duct with periodic baffles is identical in each cycle in the periodically fully developed region. The cycle average friction factor of the duct with periodic baffles is identical in each cycle, too. Therefore, the performance factor of a duct with length of $X = nL/D$ calculated from Eq. (1) is identical to the performance factor of a duct with length of $X = L/D$. The same is true on the performance factors calculated from Eqs. (3) and (4). However, it can be seen from an examination of Eq. (34) that the heat transfer rate of the duct

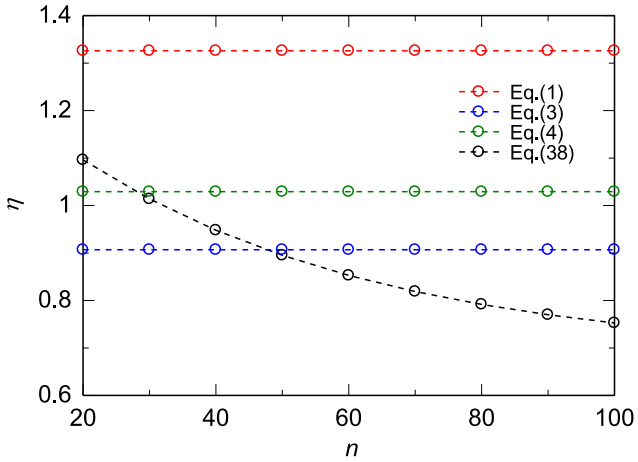

Fig. 10. Performance factor of a duct with length of $X = nL/D$ ($\mathrm{Re}_b = 438.5$).

is a function of the number of cycles, n. n is a natural number as $n = 1, 2, \cdots$. The performance factors of a duct with length of $X = nL/D$ calculated from Eqs. (1), (3), (4) and (38) under an identical pumping power for the case of $\mathrm{Re}_b = 438.5$ ($B = 30000$) are plotted in Fig. 10 as a function of the number of cycles, n. Note that the performance factors calculated from Eqs. (1), (3), (4) and (38) are discrete values at $n = 1, 2, \cdots$ not continuous values. The performance factor calculated from Eq. (38) decreases with increasing the number of cycles, n. The fluid temperature at the exit of the duct reaches the wall temperature when the duct is very long. In such a case, the heat transfer rate ratio is expressed by the mass flow rate ratio because the temperature increments from the inlet to the exit of the smooth duct and the duct with the periodic baffles are identical. Under the identical pumping power, the mass flow rate of the flow in the duct with periodic baffles is lower that of the smooth duct because of the pressure loss by the baffle plates. Therefore the performance factor takes a value below unity when the duct is long. Then, the performance factors calculated from Eqs. (1), (3) and (4) are not valid for evaluating the heat transfer enhancement and it leads to the wrong conclusion.

The term inside of the curly bracket of Eq. (34) expresses the dimensionless bulk temperature of the fluid at the exit of a cyclic circular duct of n-cycles, θ_n. That is

$$\theta_n = \frac{t_{b,n} - t_{in}}{t_w - t_{in}} = 1 - \exp\left(\frac{-4\,Nu}{\mathrm{Re}\ \mathrm{Pr}}\,\frac{nL}{D}\right) \tag{39}$$

The dimensionless bulk temperature of the fluid at the exit of a cyclic duct with baffle plates of n-cycles calculated from Eq. (39) for the case of Fig. 10 ($\mathrm{Re}_b = 438.5$ and $\mathrm{Pr} = 5$) is plotted in Fig. 11. The dimensionless bulk temperature at the exit of a smooth circular duct of the same length under the identical pumping power is also plotted in Fig. 11. The Reynolds number of the circular smooth duct under the identical pumping power is calculated from Eq. (36) as $\mathrm{Re}_s = 641.2$. The dimensionless heat transfer rate of a cyclic duct of n-cycles calculated from Eq. (34) for the case of Fig. 10 ($\mathrm{Re}_b = 438.5$ and $\mathrm{Pr} = 5$) is plotted in Fig. 12. The dimensionless heat transfer rate of a smooth circular duct of the same length under the identical pumping power is also plotted in Fig. 12.

Since the heat transfer of the duct with baffle plates is enhanced by the baffle plates, the fluid temperature of the duct with baffle plates quickly approach asymptotically to the wall temperature in comparison with the smooth duct. When the dimensionless bulk temperature of the fluid asymptotes to the wall temperature, the dimensionless heat transfer rate takes the maximum

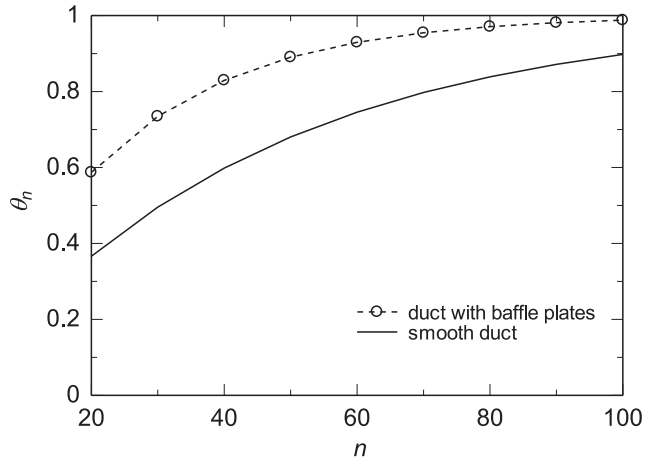

Fig. 11. Dimensionless bulk temperature at exit of cyclic circular duct of n-cycles for case of Fig. 10 ($Re_b = 438.5$ and $Re_s = 641.2$).

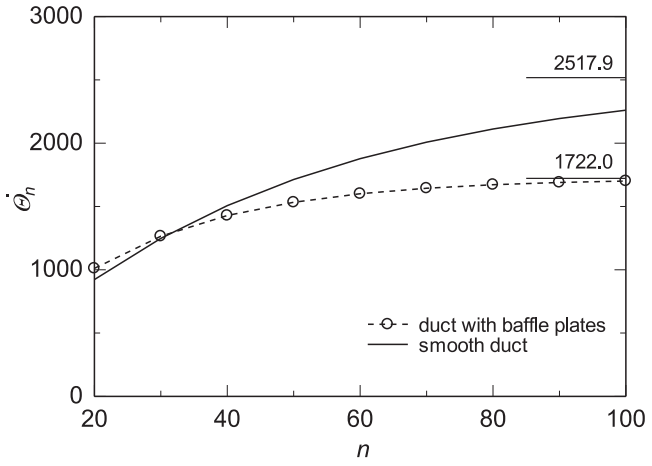

Fig. 12. Dimensionless heat transfer rate of cyclic duct of n-cycles for case of Fig. 10 ($Re_b = 438.5$ and $Re_s = 641.2$).

value and is expressed as

$$\dot{\Theta}_{max} = \frac{\pi}{4} \mathrm{Re\ Pr} \tag{40}$$

The maximum dimensionless heat transfer rate of the duct with baffle plates for the case of $Re_b = 438.5$ and $Pr = 5$ is 1722.0. In the case of the smooth duct, since the Reynolds number is $Re_s = 641.2$, the maximum dimensionless heat transfer rate is 2517.9. As seen from Fig. 12, the dimensionless heat transfer rate of the smooth duct is higher than that of the duct with baffle plates when the cycle number is greater than 30. This is the reason why the performance factor decreases with the length.

3.3. Identical mass flow rate and identical pressure drop

The performance factors under the identical mass flow rate and the identical pressure difference calculated from Eqs. (1), (3), (4) and (38) are plotted in Fig. 13(a) and (b). The St_s, Nu_s and f_s in Eqs. (1) and (3) are the Stanton number, the Nusselt number and the friction factor of the smooth duct at $Re_s = Re_b$ in the case of the identical mass flow. The St_s, Nu_s and f_s in Eqs. (1), (3) and (4) are the Stanton number, the Nusselt number and the friction factor of the smooth duct at $Re_s = B/32$ which is derived from Eq. (25) in the case of the identical pressure difference. Since Eqs. (1), (3) and (4) are derived for the flow constraint of the identical pumping power, it is obvious that there are discrepancies

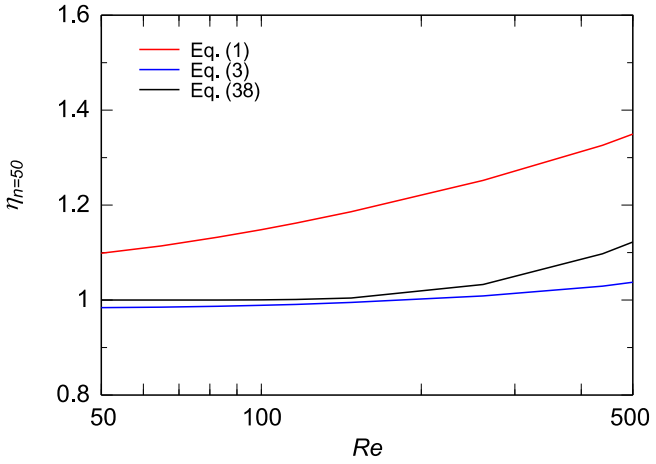

(a)

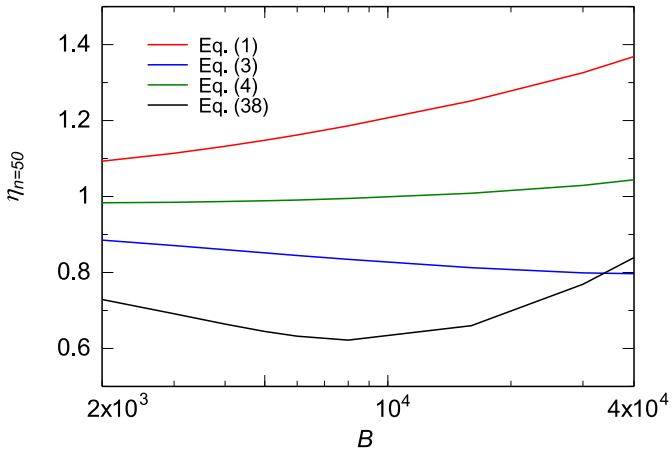

(b)

Fig. 13. Performance factor under (a) identical mass flow rate (b) identical pressure drop.

between the performance factors calculated from Eqs. (1), (3) & (4) and the performance factor calculated from Eq. (38).

4. Conclusion

The validity of the performance factors, Eq. (1), Eq. (3) and Eq. (4), which have been used in previous studies for the evaluation of heat transfer enhancement by insertion of the baffle plates under an identical pumping power, were examined. Based on that, we, therefore, made the following conclusions:

The performance factors such as Eq. (1), Eq. (3) and Eq. (4) used in previous studies are not valid for evaluating the heat transfer enhancement by insertion of baffle plates.

The direct comparison of the heat transfer rates without the assumptions of equal surface area and the equal temperature difference is suitable for evaluating heat transfer enhancement.

Declaration of Competing Interest

The authors declare that they have no known competing financial interests or personal relationships that could have appeared to influence the work reported in this paper.

CRediT authorship contribution statement

Siti Nurul Akmal Yusof: Conceptualization, Methodology, Formal analysis, Investigation, Writing – review & editing. **Nura Mu'az Muhammad:** Conceptualization, Methodology, Investigation. **Wan Mohd Arif Aziz Japar:** Conceptualization, Methodology, Investigation. **Yutaka Asako:** Conceptualization, Supervision, Methodology, Formal analysis, Investigation, Writing – original draft, Funding acquisition. **Chungpyo Hong:** Supervision, Methodology, Writing – review & editing. **Lit Ken Tan:** Supervision, Methodology, Writing – review & editing. **Nor Azwadi Che Sidik:** Supervision, Methodology, Writing – review & editing.

Acknowledgement

The authors would like to express their appreciation to Takasago Thermal Engineering Co, Ltd., Japan, for providing financial support for this work through Takasago education and research grant (Vote No: 4B631).

References

[1] R.L. Webb, E.R.G. Eckert, Application of rough surfaces to heat exchanger design, Int. J. Heat Mass Transf. 15 (1972) 1647–1658.
[2] L. Wang, B. Sunden, "Performance comparison of some tube inserts, Int. Commun. Heat Mass Transf. 29 (1) (2002) 45–56.
[3] S.W. Chang, S. Huang, Aerothermal performance of a rotating two-pass furrowed channel roughened by angled ribs, Appl. Therm. Eng. 199 (2021) 117613.
[4] Y. Yang, M. Li, Y. Zou, J. Chen, Numerical study on heat transfer characteristics of molten salt in annular channel with wire coil, Appl. Therm. Eng. 199 (2021) 117520.
[5] S.W. Chang, C. Chen, Aerothermal performances of two-pass wavy ribbed channels without and with internal effusion at three bypass angles, Int. Commun. Heat Mass Transf. 128 (2021) 105614.
[6] M.A.E. Habet, S.A. Ahmed, M.A. Saleh, Thermal/hydraulic characteristics of a rectangular channel with inline/staggered perforated baffles, Int. Commun. Heat Mass Transf. 128 (2021) 105591.
[7] S.W. Chang, P.S. Wu b, J.H. Liu, Aerothermal performance of square duct enhanced by twisted tape with inclined ribs and slots, Int. J. Heat Mass Transf. 177 (2021) 121547.
[8] G.G. Cruz, M.A.A. Mendes, J.M.C. Pereira, H. Santos, A. Nikulin, A.S. Moita, Experimental and numerical characterization of single-phase pressure drop and heat transfer enhancement in helical corrugated tubes, Int. J. Heat Mass Transf. 177 (2021) 121632.
[9] M.A. Alfellag, H.E. Ahmed, M.Gh. Jehad, M. Hameed, Assessment of heat transfer and pressure drop of metal foam-pin-fin heat sink, Int. J. Therm. Sci. 170 (2021) 107109.
[10] H. Arasteh, A. Rahbari, R. Mashayekhi, A. Keshmiri, R.B. Mahani, P. Talebizadehsardari, Effect of pitch distance of rotational twisted tape on the heat transfer and fluid flow characteristics, Int. J. Therm. Sci. 170 (2021) 106966.
[11] H. Shen, G.N. Xie, C.C. Wang, The numerical simulation with staggered alternation locations and multiflow directions on the thermal performance of double-layer microchannel heat sinks, Appl. Therm. Eng. 163 (2019) 114332.
[12] L. Liu, Z. Cao, T. Shen, L. Zhang, L. Zhang, Experimental and numerical investigation on flow and heat transfer characteristics of a multi-waves internally spiral finned tube, Int. J. Heat Mass Transf. 167 (2021) 107030.
[13] Y. Lv, Z. Wen, Q. Li, Y. Qiu, Numerical investigation on thermal hydraulic performance of hybrid wavy channels in a supercritical CO 2 precooler, Int. J. Heat Mass Transf. 181 (2021) 121891.
[14] Y. Asako, M. Faghri, Finite-volume solutions for laminar flow and heat transfer in a corrugated duct, Trans. ASME: J. Heat Transf. 109 (1987) 627–634.
[15] N.M. Muhammad, W.M.A.A. Japar, S.N.A. Yusof, Y. Asako, M. Faghri, L.K. Tan, N.A.C. Sidik, Validity of performance factors used in recent studies on heat transfer enhancement of nanofluids, Trans. ASME: J. Heat Transf. 143 (8) (2021) 084501.
[16] S.V. Patankar, C.H. Liu, E.M. Sparrow, Fully developed flow and heat transfer in ducts having streamwise periodic variation of cross sectional area, Trans. ASME: J.Heat Transf. 99 (1977) 180–186.
[17] Y.A. Cengel, A.J. Ghajar, Heat and Mass Transfer : Fundamentals and Applications, McGraw-Hill Education, New York, 2005 (ISBN: 978-981-4595-27-8).
[18] M.M. Zdravkovich, Flow Around Circular cylinders, Fundamentals, vol. 1, Oxford University Press, Oxford, 1997.
[19] S.V. Patankar, Numerical Heat Transfer and Fluid Flow, Hemisphere Publishing Corporation, New York, 1980 (ISBN: 0-89116-522-3).
[20] S.V. Patankar, Computation of Conduction and Duct Flow Heat Transfer, Innovative Research, Inc., Minnesota, 1991.